

# d-wave and $s^\pm$ Pairing Strengths in $\text{Ba}_2\text{CuO}_{3+\delta}$

T. A. Maier,<sup>1,2</sup> T. Berlijn,<sup>1,2</sup> and D. J. Scalapino<sup>3</sup>

<sup>1</sup>Computational Sciences and Engineering Division,

Oak Ridge National Laboratory, Oak Ridge, Tennessee 37831, USA

<sup>2</sup>Center for Nanophase Materials Sciences, Oak Ridge National Laboratory, Oak Ridge, TN 37831, USA

<sup>3</sup>Department of Physics, University of California, Santa Barbara, CA 93106-9530, USA

(Dated: April 7, 2024)

Using a first principles derived two-orbital model ( $d_{x^2-y^2}$ ,  $d_{3z^2-r^2}$ ) and a random phase approximation treatment of the spin-fluctuation pairing vertex, we calculate the  $d$ -wave and  $s^\pm$ -wave pairing strengths for a model of the recently discovered  $\text{Ba}_2\text{CuO}_{3+\delta}$  superconductor. We find that there is significant pairing strength in both of these channels. These results provide an interesting perspective on the relationship between the cuprates and Fe-based superconductors and the high- $T_c$  pairing mechanism.

In 2009, Geballe and Marezio [1] published a review of superconductivity in  $\text{Sr}_2\text{CuO}_{4-x}$  [2, 3] in which they noted that, while it was isostructured to the familiar 214  $\text{La}_2\text{CuO}_4$  system, it was extremely overdoped and had a superconducting transition temperature of  $T_c = 95$  K, which was more than twice that of optimally doped  $\text{La}_{1.84}\text{Sr}_{0.16}\text{CuO}_4$ . Since that time bulk superconductivity at  $T_c = 84$  K in  $\text{Cu}_{0.75}\text{Mo}_{0.25}\text{Sr}_2\text{YCu}_2\text{O}_{7.54}$  [4] and exceeding 70 K in  $\text{Ba}_2\text{CuO}_{3+\delta}$  [5] have been reported. All of these materials have been synthesized at high temperatures and pressures in the presence of a strong oxidizing agent. They are characterized as highly overdoped with a reduced Cu apical O spacing compared to typical cuprate superconductors. Here, using a two-orbital ( $d_{x^2-y^2}$ ,  $d_{3z^2-r^2}$ ) tight-binding model derived from first principles for a single layer of  $\text{Ba}_2\text{CuO}_4$  and a multi-orbital random phase approximation (RPA) calculation [6, 7] of the pairing vertex, we find that there is both significant  $A_{1g}(d_{x^2-y^2})$  and  $B_{1g}(s^\pm)$  pairing strength in this overdoped cuprate material with a compressed octahedron structure.

The density functional theory (DFT) bandstructure for a single layer of  $\text{Ba}_2\text{CuO}_4$  is shown in Fig. 1a. A Wannier transformation to a 2-orbital  $\text{Cu}-(d_{x^2-y^2}, d_{3z^2-r^2})$  model gives the two bands illustrated in Fig. 1a. The Fermi surface assuming a rigid band shift for  $\text{Ba}_2\text{CuO}_{3.5}$  is shown in Fig. 1b. It consists of an electron-like sheet with majority  $d_{3z^2-r^2}$  orbital weight around the zone center  $\Gamma$  and a hole-like sheet with majority  $d_{x^2-y^2}$  orbital weight around the  $(\pi, \pi)$  point of the 2D Brillouin zone. The two orbital Wannier function based Hamiltonian is given by

$$H_0 = \sum_{k\sigma} \sum_{\ell\ell'} (\xi_{\ell\ell'}(k) + (\varepsilon_\ell - \mu) \delta_{\ell\ell'}) d_{\ell\sigma}^\dagger(k) d_{\ell'\sigma}(k) \quad (1)$$

Here  $\ell = 1$  denotes the  $d_{x^2-y^2}$  orbital and  $\ell = 2$  the  $d_{3z^2-r^2}$  orbital. The tight-binding parameters and the technical details of the first principles calculations are given in the Supplementary Material. For the Fermi surfaces shown in Fig. 1b, the chemical potential  $\mu$  has been adjusted to give a doping  $\delta = 0.5$ . The onsite interaction

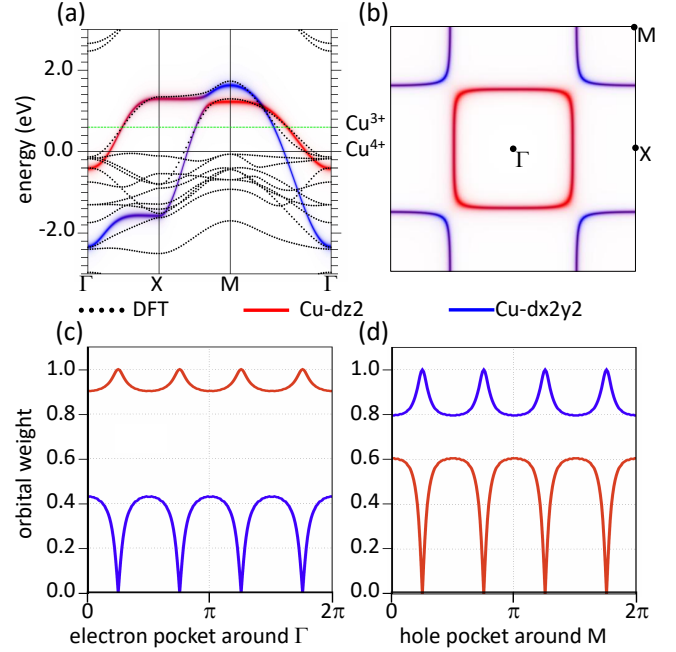


FIG. 1: (Color online) (a) The two-orbital Wannier function and Density Functional Theory (DFT) bandstructures of  $\text{Ba}_2\text{CuO}_4$ . The green line corresponds to a rigid band shift filling for  $\text{Ba}_2\text{CuO}_{3.5}$ . (b) The Fermi surface for this filling with the orbital weight for  $d_{x^2-y^2}$  (blue) and  $d_{3z^2-r^2}$  (red). (c) and (d)  $d_{x^2-y^2}$  and  $d_{3z^2-r^2}$  orbital weights plotted versus the angle as  $k$  varies around the Fermi surfaces.

part of the Hamiltonian has the usual form

$$\begin{aligned} H_1 = & U \sum_{i,\ell} n_{i\ell\uparrow} n_{i\ell\downarrow} + U' \sum_{i,\ell' < \ell} n_{i\ell} n_{i\ell'} \\ & + J \sum_{i,\ell' < \ell\sigma,\sigma'} \sum_{\sigma} d_{i\ell\sigma}^\dagger d_{i\ell'\sigma'}^\dagger d_{i\ell\sigma'} d_{i\ell'\sigma} \\ & + J' \sum_{i,\ell' \neq \ell} d_{i\ell}^\dagger d_{i\ell\downarrow}^\dagger d_{i\ell'\downarrow} d_{i\ell'\uparrow}. \end{aligned} \quad (2)$$

A similar 2-orbital ( $d_{x^2-y^2}$ ,  $d_{3z^2-r^2}$ ) Hamiltonian has been used by Jiang et al. [8] to model a  $\text{CuO}_2$  monolayer

on Bi2212 [9]. Here too the  $\text{CuO}_2$  monolayer is heavily overdoped by charge transfer at the interface and has a short Cu apical bond to the O in the substrate. Treating this model using a Gutzwiller approximation, they derived a spin-orbit superexchange pairing interaction of the Kugel-Kohmskii form and find nodeless  $A_{1g}$   $s^\pm$  pairing.

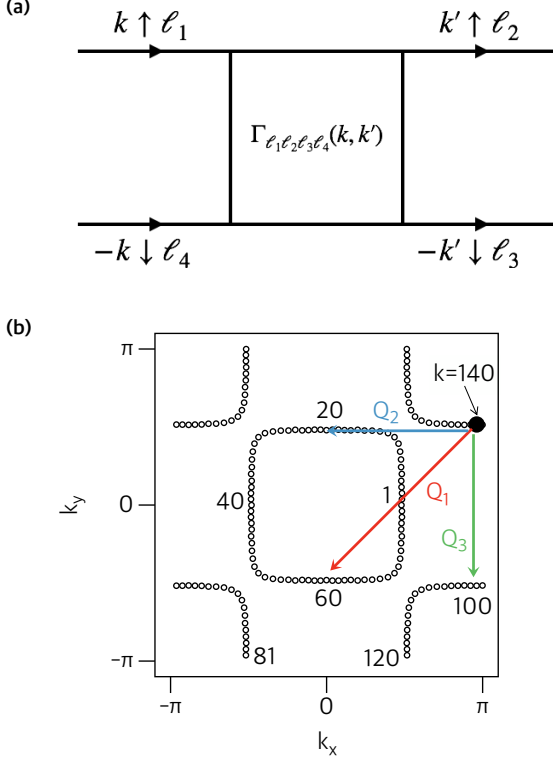


FIG. 2: (Color online) (a) The scattering vertex  $\Gamma_{\ell_1\ell_2\ell_3\ell_4}(k, k')$  and (b) The point  $k = 140$  is fixed at the bottom of the hole band and  $k'$  varies along the Fermi surfaces. The peaks in the vertices  $\Gamma_{\ell_1\ell_2\ell_3\ell_4}(k, k')$  shown in Fig. 3 at  $k' = 60$  and the smaller ones at 20 and 100 arise from the  $k' - k$  scattering labeled  $Q_1$ ,  $Q_2$  and  $Q_3$ , respectively.

In the multi-orbital RPA theory the pairing vertex  $\Gamma_{\ell_1\ell_2\ell_3\ell_4}(k, k')$  for scattering a singlet pair ( $k \uparrow \ell_1, -k \downarrow \ell_4$ ) in orbitals  $\ell_1$  and  $\ell_4$  to ( $k' \uparrow \ell_2, -k' \downarrow \ell_3$ ) in orbitals  $\ell_2$  and  $\ell_3$  is given by

$$\begin{aligned} \Gamma_{\ell_1\ell_2\ell_3\ell_4}(k, k') = & \left[ \frac{3}{2} U^s \chi_S^{\text{RPA}}(k - k') U^s \right. \\ & - \frac{1}{2} U^c \chi_O^{\text{RPA}}(k - k') U^c \\ & \left. + \frac{1}{2} (U^s + U^c) \right]_{\ell_1\ell_2\ell_3\ell_4} \end{aligned} \quad (3)$$

Here  $U^s$  and  $U^c$  represent  $4 \times 4$  matrices in orbital space which depend on the interaction parameters and  $\chi_S^{\text{RPA}}$  and  $\chi_O^{\text{RPA}}$  are orbital matrix RPA spin and orbital

(charge) susceptibilities given in the Supplementary Material.

In the following we will consider two sets of interaction parameters, the first of which ( $U = 1, U' = 0.5, J = J' = 0.25$ ) satisfies rotational invariance and the second ( $U = U' = 0.8, J = J' = 0.4$ ) of which does not. These interaction parameters like the tight-binding parameters given in the Supplemental Material are given in eV. We will find for both sets that the  $B_{1g}$  ( $d$ -wave) and  $A_{1g}$  ( $s$ -wave) pairing strengths are similar. For the first parameter set the  $B_{1g}$  strength is larger than that of the  $A_{1g}$  channel but for the second parameter set the close balance between these two is tipped in favor of the  $A_{1g}$  channel.

The dominant orbital scattering vertices for the two different interaction parameter sets are shown in Fig. 3a and 3b.

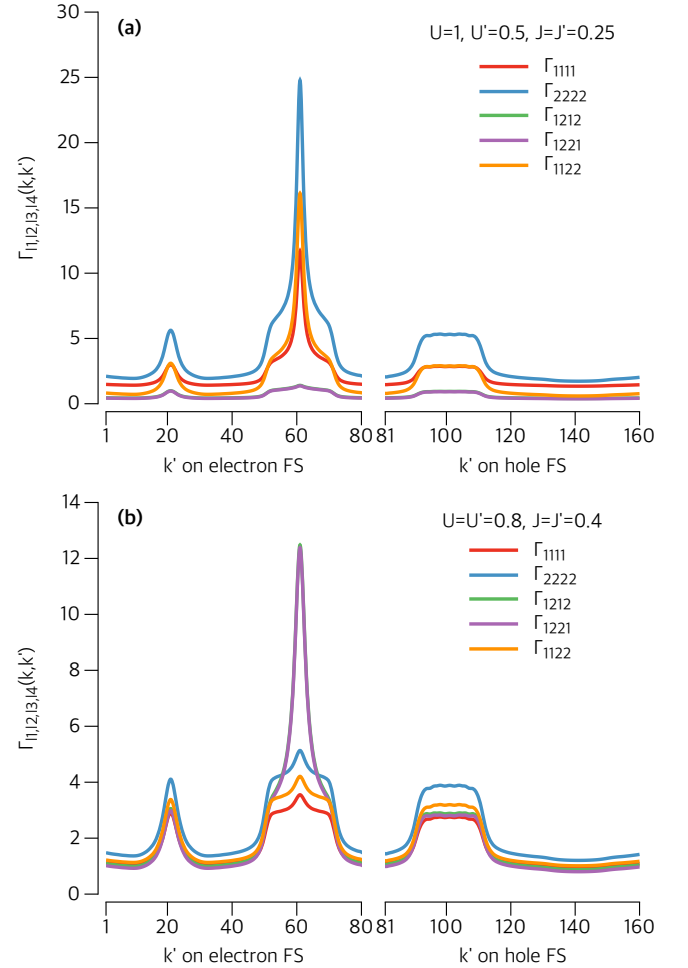


FIG. 3: (Color online) Selected orbital dependent vertices  $\Gamma_{1111}(k, k')$ ,  $\Gamma_{2222}(k, k')$ ,  $\Gamma_{1212}(k, k')$  and  $\Gamma_{1221}(k, k')$ ,  $\Gamma_{1122}(k, k')$  for (a)  $U = 1.0, U' = 0.5, J = J' = 0.25$  and  $T = 0.06$ , and (b)  $U = U' = 0.8, J = J' = 0.4$  and  $T = 0.1$ . In this case the  $U'$  and  $J'$  dependent scattering  $\Gamma_{1221}(k, k')$  is largest.

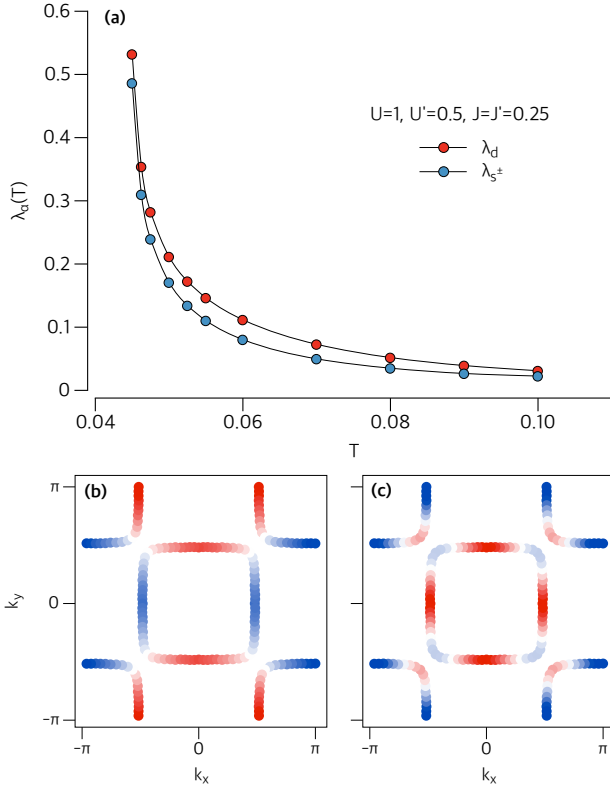


FIG. 4: (Color online) (a) The pairing strength eigenvalues  $\lambda_d(T)$  and  $\lambda_{s\pm}(T)$  versus temperature  $T$  for  $U = 1.0, U' = 0.5, J = J' = 0.25$ . The gap eigenfunctions  $g_d(k)$  on the Fermi surface (b) for the  $d$ -wave at  $T = 0.06$  and (c) for the  $s^\pm$ -wave at  $T = 0.1$ .

Here  $k$  is fixed at the bottom of the hole Fermi surface that surrounds the  $M$  point and  $k'$  varies over the electron Fermi surface over points 1–80 and then over the hole Fermi surface points 81 to 160 as shown in Fig. 2b. As shown in Fig. 3a for the rotationally invariant parameter set, the dominant contribution to the pairing is associated with the orbital vertices  $\Gamma_{1111}, \Gamma_{2222}, \Gamma_{1122}, \Gamma_{2211}$  in which the spin-up and spin-down electrons remain in the same orbital states. In leading order these scattering processes involve  $U$  and  $J$ . In addition, there are scattering processes which involve an orbital change such as  $\Gamma_{1221}$  in which a pair in orbital  $d_{x^2-y^2}$  scatters to a pair in orbital  $d_{3z^2-r^2}$  or  $\Gamma_{1212}$  in which a pair ( $k \uparrow 1, -k \downarrow 2$ ) scatters to ( $k \uparrow 2, -k \downarrow 1$ ). These scattering processes involve  $U'$  and  $J'$  and become significant for the second set of parameters shown in Fig. 3b where the inter-orbital exchange  $J'$  is larger.

Using these scattering vertices, the pairing strength is given by the eigenvalue of

$$-\sum_j \oint \frac{dk'_\parallel}{2\pi v_{Fj}(k'_\parallel)} \Gamma_{ij}(k, k') g_j^\alpha(k') = \lambda_\alpha g_i^\alpha(k) \quad (4)$$

with

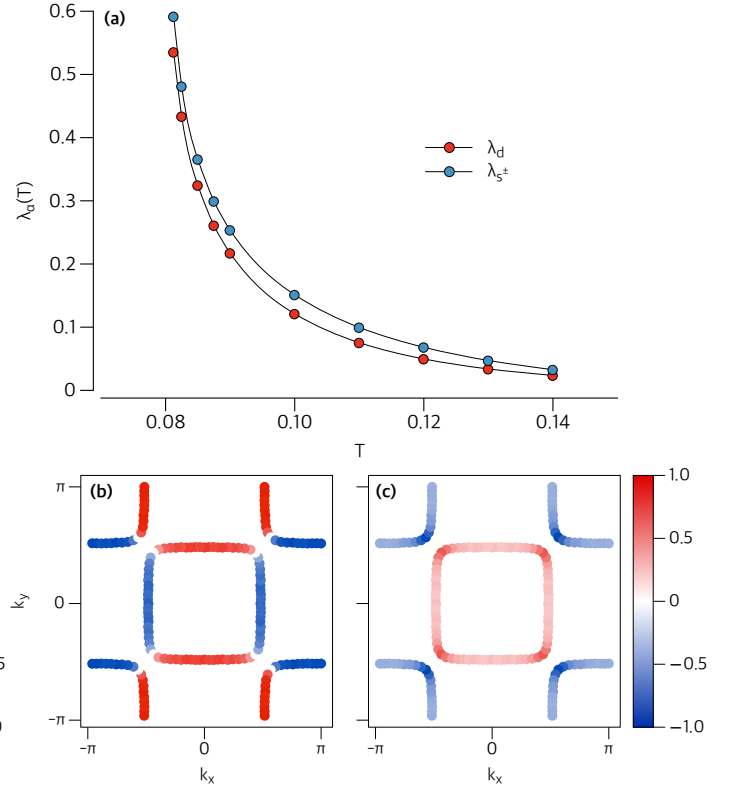


FIG. 5: (Color online) (a) The pairing strength eigenvalues  $\lambda_d(T)$  and  $\lambda_{s\pm}(T)$  versus temperature  $T$  for  $U = U' = 0.8, J = J' = 0.4$ . The  $d$ -wave eigenfunction for  $T = 0.06$  and  $s^\pm$ -wave eigenfunction for  $T = 0.1$  on the Fermi surface are shown in (b) and (c) respectively.

$$\Gamma_{ij}(k, k') = \sum_{\ell_1 \ell_2 \ell_3 \ell_4} a_{\nu_i}^{\ell_1}(k) a_{\nu_i}^{\ell_4}(-k) \Gamma_{\ell_1 \ell_2 \ell_3 \ell_4}(k, k') \times a_{\nu_j}^{\ell_2*}(k') a_{\nu_j}^{\ell_3*}(-k') \quad (5)$$

Here  $j$  sums over the Fermi surfaces and  $v_{Fj}(k'_\parallel)$  is the Fermi velocity  $|\nabla_k E_{\nu_j}(k)|$ . The pairing strength eigenvalues for the  $B_{1g}$  ( $d$ -wave) and  $A_{1g}$  ( $s^\pm$ -wave) along with the eigenfunctions  $g_\alpha(k)$  which reflect the expected structure of the superconducting gap are plotted in Fig. 4 and Fig. 5 for the two parameters sets.

In both cases the pairing strengths for the  $B_{1g}$  ( $d$ -wave) and the  $A_{1g}$  ( $s^\pm$ -wave) are quite close to each other. As seen in Fig. 2b, the dominant pair scattering process for momentum transfer  $(\pi, \pi)$  involves the scattering shown as  $Q_1$  which contributes positively to the pairing strength in both the  $d$ -wave and  $s^\pm$  channels. Similarly the scattering  $Q_2$  contributes positively to both, while the scattering at  $Q_3$  contributes negatively. The difference between the two channels is tipped by a decrease in  $U$  and an increase in  $J'$ .

To conclude, in a two-orbital ( $3d_{x^2-y^2}, 3d_{3z^2-r^2}$ ) RPA model of  $\text{Ba}_2\text{CuO}_{3+\delta}$  we find pairing strength in both

the  $B_{1g}$  ( $d$ -wave) and  $A_{1g}$  ( $s$ -wave) channels, with the  $d$ -wave channel favored for rotationally invariant interaction parameters. The pairing strength is large relative to a similar calculation for an optimally doped single-band Hubbard model. This is in spite of the two orbitals each having significant orbital weight at the Fermi energy. This appears counter to previous calculations which have concluded that  $T_c$  is optimized when the orbital weight is concentrated in a single  $3d_{x^2-y^2}$  orbital [10, 11]. However, these calculations also found that the pairing strength depended upon the shape of the Fermi surface and in the present case, the nearly square shapes of both the electron and hole Fermi surfaces are responsible for the enhanced pairing strength. We believe that this is what is responsible for the second superconducting dome in the highly overdoped region of the cuprate phase diagram proposed by Geballe and Marezio [1].

The occurrence of two pairing channels in this overdoped cuprate regime is reminiscent of  $Ba_{0.6}K_{0.4}Fe_2As_2$ . In that case, below  $T_c$  an emergent  $B_{1g}$  ( $d$ -wave) mode is observed in Raman scattering [12]. This has been interpreted as arising from a Bardasis-Schrieffer mode associated with a subdominant  $d_{x^2-y^2}$  pairing channel in an  $s^\pm$  superconductor. In the  $Ba_2CuO_{3+\delta}$  case, one could have a  $d$ -wave superconductor with a subdominant  $s^\pm$  mode. The Raman observation of such behavior would provide an interesting link between the cuprate and Fe-based superconductors.

### Acknowledgments

The possibility of another region of superconductivity in the extremely overdoped cuprates was proposed to one of us by Theodore H. Geballe a number of years ago. The DFT calculations, the derivation of the tight-binding model (TB) and the analysis of the results (DJS) were supported by the Scientific Discovery through Advanced Computing (SciDAC) program funded by U.S. Department of Energy, Office of Science, Advanced Scientific

Computing Research and Basic Energy Sciences, Division of Materials Sciences and Engineering. The RPA calculations (TAM) were supported by the U.S. Department of Energy, Office of Basic Energy Sciences, Materials Sciences and Engineering Division.

- 
- [1] T. H. Geballe and M. Marezio, *Physica C* **469**, 680 (2009).
  - [2] Q. Q. Lin, H. Yang, X.M. Qin, Y.Yu, L.X. Yang, F.Y.Li, R.C.Yu, C.Q.Jin, S.Uchida, *Phys. Rev. B* **74**, 100506 (2006).
  - [3] Z. Hiroi, M. Takano, M. Azuma, Y. Takeda, *Nature* **364**, 315 (1993).
  - [4] A. Gauzzi, Y. Klein, M. Nisula, M. Karppinen, P. K. Biswas, H. Saadaoui, E. Morenzoni, P. Manuel, D.Khalyavin, M. Marezio, and T. H. Geballe, *Phys. Rev. B* **94**, 180509 (R) (2016).
  - [5] W. M. Li, L. P. Cao, J. F. Zhao, R. Z. Yu, J. Zhang, Y. Liu, Q. Q. Liu, G. Q. Zhao, X. C. Wang, Z. Hu, Q. Z. Huang, H. Wu, H. J. Lin, C. T. Chen, J. S. Kim, G. Steward, Z. Li, Y. W. Long, Z. Z. Gong, Z. Guguchia, Y. J. Uemura, S. Uchida, C. Q. Jin, *preprint* arXiv:1808.09425 (2018).
  - [6] K. Kubo, *Phys. Rev. B*, **75**, 224509 (2007).
  - [7] A. F. Kemper, T. A. Maier, S. Graser, P. J. Hirschfeld, D. J. Scalapino, *New J. Phys.* **12**, 073030 (2010).
  - [8] K. Jiang, X. Wu, J. Hu and Z. Wang, *preprint* arXiv:1804.05072 (2018).
  - [9] Y. Zhong, Y. Wang, S. Han, Y.-F. Lv, W.-L. Wang, D. Zhang, H. Ding, Y.-M. Zhang, L. Wang, K. He, R. Zhong, J. A. Schneeloch, G.-D. Gu, C.-L. Song, X.-C. Ma, Q.-K. Xue, *Science Bulletin* **61**, 1239 (2016).
  - [10] E. Pavarini, I. Dasgupta, T. Saha-Dasgupta, O. Jepsen, O. K. Anderson, *Phys. Rev. Lett.* **87**, 047003 (2001).
  - [11] H. Sakakibara, K. Suzuki, H. Usui, K. Kuroki, R. Arita, D.J.Scalapino, H. Aoki, *Physics Procedia* **45**, 13 (2013).
  - [12] T. Bhm, A. F. Kemper, B. Moritz, F. Kretschmar, B. Muschler, H.-M. Eiter, R. Hackl, T. P. Devereaux, D.J. Scalapino, and H.-H. Wen, *Phys. Rev. X* **4**, 041046 (2014).

# **$d$ -wave and $s^\pm$ Pairing Strengths in $\text{Ba}_2\text{CuO}_{3+\delta}$ - Supplementary Material**

T. A. Maier and T. Berlijn

*Computational Sciences and Engineering Division,  
Oak Ridge National Laboratory, Oak Ridge, Tennessee 37831, USA and  
Center for Nanophase Materials Sciences,  
Oak Ridge National Laboratory, Oak Ridge, TN 37831, USA*

D. J. Scalapino

*Department of Physics, University of California,  
Santa Barbara, CA 93106-9530, USA*

(Dated: April 7, 2024)

To derive the two-orbital Wannier function based Hamiltonian of  $\text{Ba}_2\text{CuO}_{3+\delta}$  we performed Density Functional Theory (DFT) calculations. To that end we applied the WIEN2K[1] implementation of the full potential linearized augmented plane wave method within the generalized gradient approximation using the PBE exchange correlation functional. [2]. First we performed a calculation of bulk  $\text{Ba}_2\text{CuO}_4$  in which the space group  $I4/mmm$  and the lattice constants  $a = 7.5646$  Bohr and  $c = 24.4568$  Bohr were taken from Ref. [3] and in which the internal forces on the atoms were relaxed to less than 2 mRy/Bohr. The theoretically obtained apical O height of 3.65 Bohr compares well with the experimental value of 3.51 Bohr reported in Ref. [3]. We used the theoretically obtained Ba and apical O heights together with the experimental in-plane lattice constant  $a = 7.5646$  Bohr to build a  $\text{Ba}_2\text{CuO}_4$  monolayer with a vacuum of roughly 37 Bohr. A Wannier transformation of the monolayer calculation was performed with the `wien2wannier` and `Wannier90` software. [4, 5] Specifically a Wannier transformation was performed in which the  $\text{Cu-}x^2 - y^2$  and  $\text{Cu-}z^2$  orbitals were projected on the bands within  $[-3.5, 2]$  eV and in which the following `Wannier90` parameters were used `num_iter=0`, `dis_num_iter=1000`, `dis_froz_min=0.5` and `dis_froz_min=2.5`. The elements of the resulting Wannier function based Hamiltonian were rounded up to the nearest meV, cut beyond 3rd nearest neighboring Cu atoms and are summarized in Tab. I. Here, the orbital matrices are labeled by  $(\ell_1, \ell_2)$  with  $\ell = 1$  for the  $d_{x^2-y^2}$  orbital and  $\ell = 2$  for the  $d_{3z^2-r^2}$  orbital. The k-point mesh was taken to be  $5 \times 5 \times 5$  for the bulk DFT calculation,  $10 \times 10 \times 1$  for the monolayer DFT calculation and  $5 \times 5 \times 1$  for the monolayer Wannier transformation. The basis set sizes of the DFT calculations were determined by `RKmax=7`.

TABLE I: Hopping parameters of the first principles Wannier function based Hamiltonian of  $\text{Ba}_2\text{CuO}_4$  in eV.

	on-site energy	1 <sup>st</sup> ( $t$ )	2 <sup>nd</sup> ( $t'$ )	3 <sup>rd</sup> ( $t''$ )
intra-orbital $d_{x^2-y^2}$	$\varepsilon_1 = 0.624$	$t_{11} = -0.495$	$t'_{11} = 0.057$	$t''_{11} = -0.099$
intra-orbital $d_{3z^2-r^2}$	$\varepsilon_2 = -0.185$	$t_{22} = -0.205$	$t'_{22} = -0.016$	$t''_{22} = -0.039$
inter-orbital	0	$t_{12} = 0.318$	$t'_{12} = 0$	$t''_{12} = 0.067$

With these parameters, the dispersions  $\xi_{\ell\ell'}(k)$  entering the Hamiltonian  $H_0$  in Eq. (1) are

$$\begin{aligned}\xi_{11/22}(k) &= 2t_{11/22}(\cos k_x + \cos k_y) + 4t'_{11/22} \cos k_x \cos k_y \\ &\quad + 2t''_{11/22}(\cos 2k_x + \cos 2k_y) \\ \xi_{12}(k) = \xi_{21}(k) &= 2t_{12}(\cos k_x - \cos k_y) + 2t''_{12}(\cos 2k_x - \cos 2k_y)\end{aligned}\quad (\text{S1})$$

This Hamiltonian is then supplemented by the interaction terms given in Eq. (2) of the main text. The interaction matrices in the orbital basis (11, 22, 12, 21) are

$$\begin{aligned}U^S &= \begin{pmatrix} U & J & 0 & 0 \\ J & U & 0 & 0 \\ 0 & 0 & U' & J' \\ 0 & 0 & J' & U' \end{pmatrix} \\ U^C &= \begin{pmatrix} U & 2U' - J & 0 & 0 \\ 2U' - J & U & 0 & 0 \\ 0 & 0 & -U' + 2J & J' \\ 0 & 0 & J' & -U' + 2J \end{pmatrix}.\end{aligned}\quad (\text{S2})$$

The RPA spin  $\chi_S^{\text{RPA}}$  and charge  $\chi_O^{\text{RPA}}$  susceptibilities are

$$\begin{aligned}\chi_S^{\text{RPA}}(q) &= [1 - U^S \chi^0(q)]^{-1} \chi^0(q) \\ \chi_O^{\text{RPA}}(q) &= [1 - U^C \chi^0(q)]^{-1} \chi^0(q)\end{aligned}\quad (\text{S3})$$

where the matrix elements of the bare susceptibility  $\chi^0(q)$  are given by

$$\chi_{\ell_1 \ell_2 \ell_3 \ell_4}^0(q, \omega_m) = -\frac{T}{N} \sum_{k, \omega_n} G_{\ell_3 \ell_1}^0(k + q, \omega_n + \omega_m) G_{\ell_2 \ell_4}^0(k, \omega_n) \quad (\text{S4})$$

with  $G_{\ell\ell'}^0(k, \omega_n)$  the bare Green's function

$$G_{\ell\ell'}^0(k, \omega_n) = \sum_{\mu} \frac{a_{\mu}^{\ell}(k) a_{\mu}^{\ell'*}(k)}{i\omega_n - \xi_{\mu}(k)}. \quad (\text{S5})$$

Typically the largest terms in the bare susceptibility are the diagonal  $\chi_{1111}^0$ ,  $\chi_{2222}^0$ ,  $\chi_{1212}^0$  and  $\chi_{2121}^0$  terms and as a consequence  $\Gamma_{1111}$ ,  $\Gamma_{2222}$ ,  $\Gamma_{1122}$  and  $\Gamma_{2211}$  depend on the upper lefthand quadrant  $U$ ,  $J$  terms of the interaction while  $\Gamma_{1212}$ ,  $\Gamma_{1221}$ , etc. depend upon  $U'$  and  $J'$ . All of the orbital vertices  $\Gamma_{\ell_1 \ell_2 \ell_3 \ell_4}(k, k')$  are shown in Figures S1a and S1b for the two sets of interaction parameters that we have studied. Here one can see that the dominant

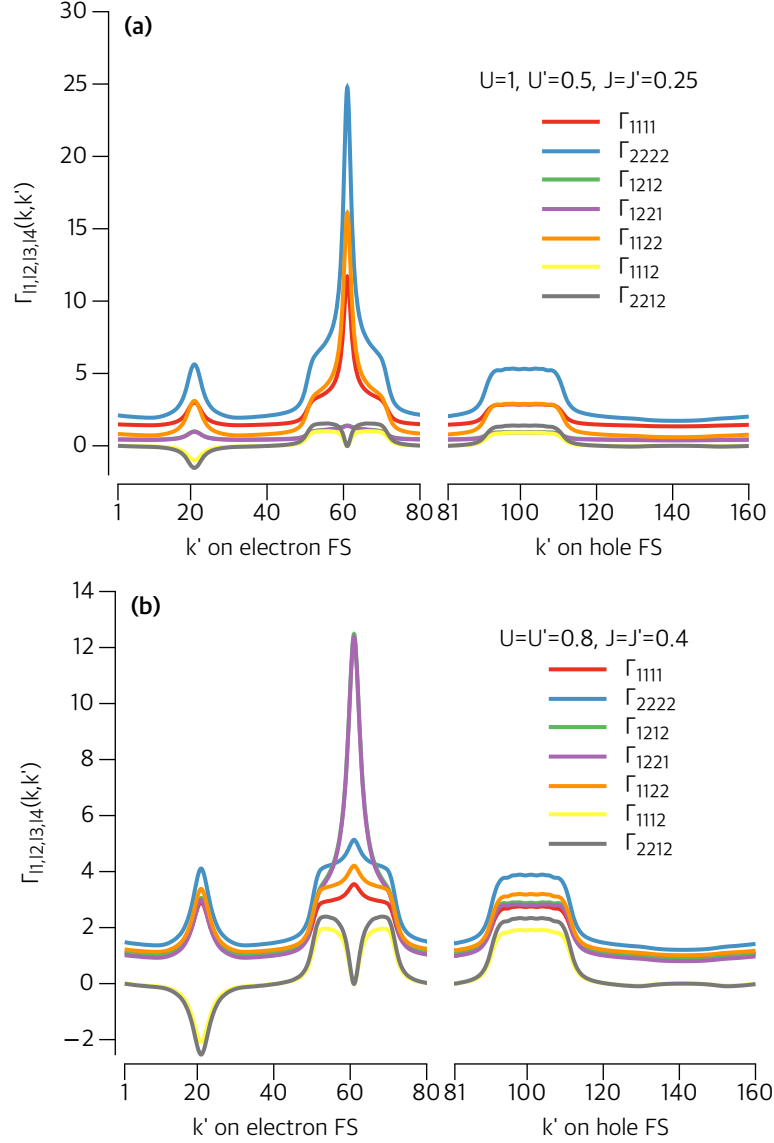


FIG. S1: (Color online) The orbital vertices  $\Gamma_{\ell_1\ell_2\ell_3\ell_4}(k, k')$  for  $k$  fixed as shown in Fig. 2(b) and  $k'$  varying along the electron and hole Fermi surfaces. (a)  $U = 1.0$ ,  $U' = 0.5$ ,  $J = J' = 0.25$ ,  $T = 0.06$  and (b)  $U = U' = 0.8$ ,  $J = J' = 0.4$ ,  $T = 0.1$ .

vertices are those shown in Figs. 2 and 3.

As discussed in the text, the  $\Gamma_{1212}$  and  $\Gamma_{1221}$  vertices involve the exchange of a fluctuation in which the orbital quantum number of the up and down spins changes. In this case, the spin fluctuations which contribute to the pairing are in the inter-orbital spin susceptibility channel. For example,

$$\chi_{1212}(q, \omega_m) = \int_0^\beta d\tau e^{-i\omega_m\tau} \langle \mathcal{T}_\tau m_{21}(q, \tau) m_{21}^\dagger(q, 0) \rangle \quad (\text{S6})$$



with

$$m_{21}^\dagger(q) = \frac{1}{\sqrt{N}} \sum_k d_{2\uparrow}^\dagger(k+q) d_{1\downarrow}(k) \quad (\text{S7})$$

RPA results showing this inter-orbital spin susceptibility

$$\chi_{\text{inter}}(q) = \chi_{1212}(q, \omega_m = 0) + \chi_{2121}(q, \omega_m = 0) \quad (\text{S8})$$

are plotted in Fig. S2a and Fig. S2b for the two parameter sets we have studied. RPA results for the usual intra-orbital spin susceptibility are also shown. For the second set of interaction parameters the inter-orbital spin susceptibility is clearly important. These fluctuations would not be seen in neutron scattering.

Results for the pair eigenfunctions  $g_d(k)$  and  $g_{s^\pm}(k)$  versus  $k$  are shown in Fig. S3 for the two parameter sets discussed in our paper. For the  $U = 1.0$  parameter set, the  $s^\pm$  eigenfunction has 8 nodes, but for the  $U = 0.8$  parameter set it is nodeless.

---

- [1] P. Blaha *et al.*, Comput. Phys. Commun. **147**, 71 (2002).
- [2] J. P. Perdew, K. Burke and M. Ernzerhof, Phys. Rev. Lett. **77**, 3865 (1996).
- [3] W. M. Li *et al.*, arXiv:1808.09425 (2018)
- [4] J. Kunes, R. Arita, P. Wissgott, A. Toschi, H. Ikeda, and K. Held, Comp. Phys. Commun. **181**, 1888 (2010).
- [5] A. A. Mostofi, J. R. Yates, G. Pizzi, Y. S. Lee, I. Souza, D. Vanderbilt and N. Marzari Comput. Phys. Commun. **185**, 2309 (2014).

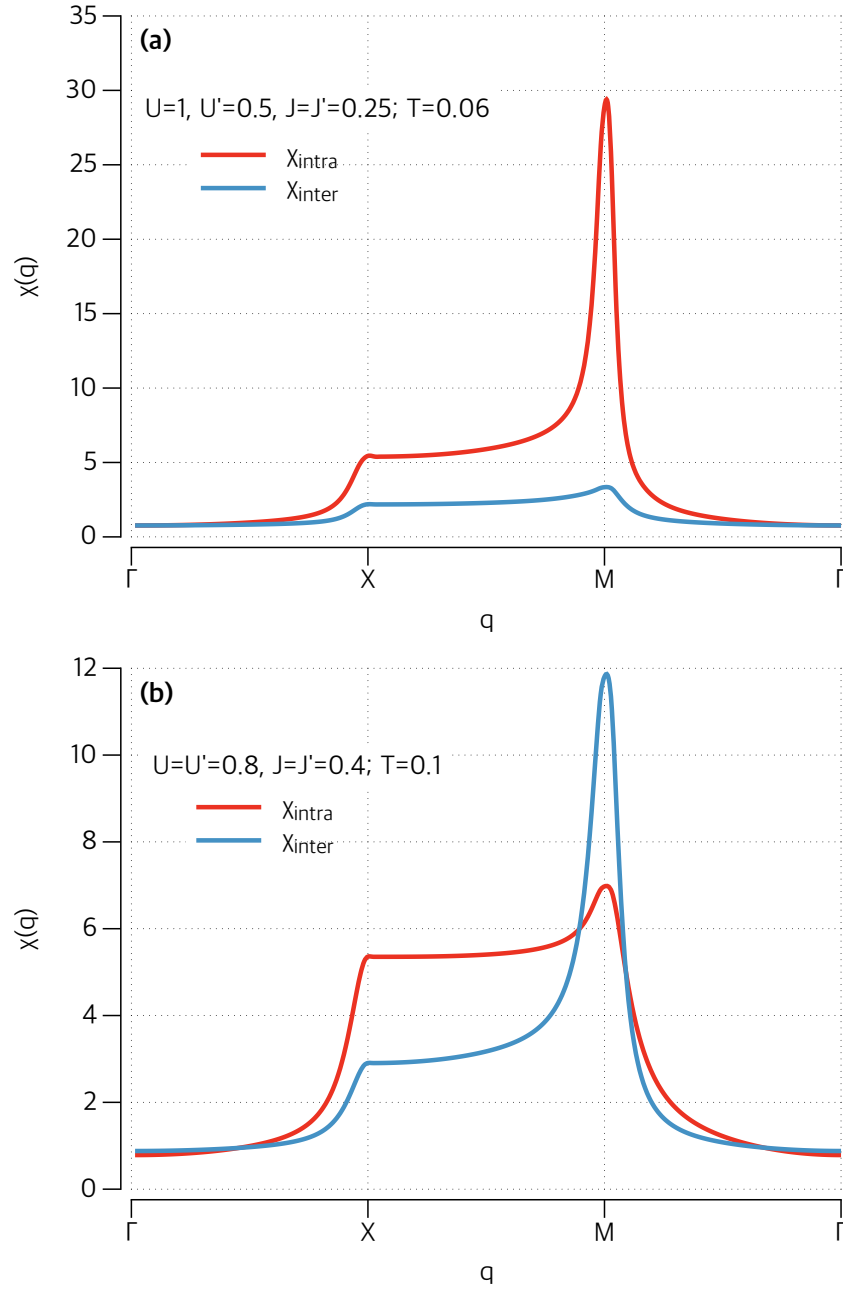


FIG. S2: (Color online) The intra- and inter-spin susceptibility for (a)  $U = 1.0$ ,  $U' = 0.5$ ,  $J = J' = 0.25$  and  $T = 0.06$ , and (b)  $U = U' = 0.8$ ,  $J = J' = 0.4$  and  $T = 0.1$ .

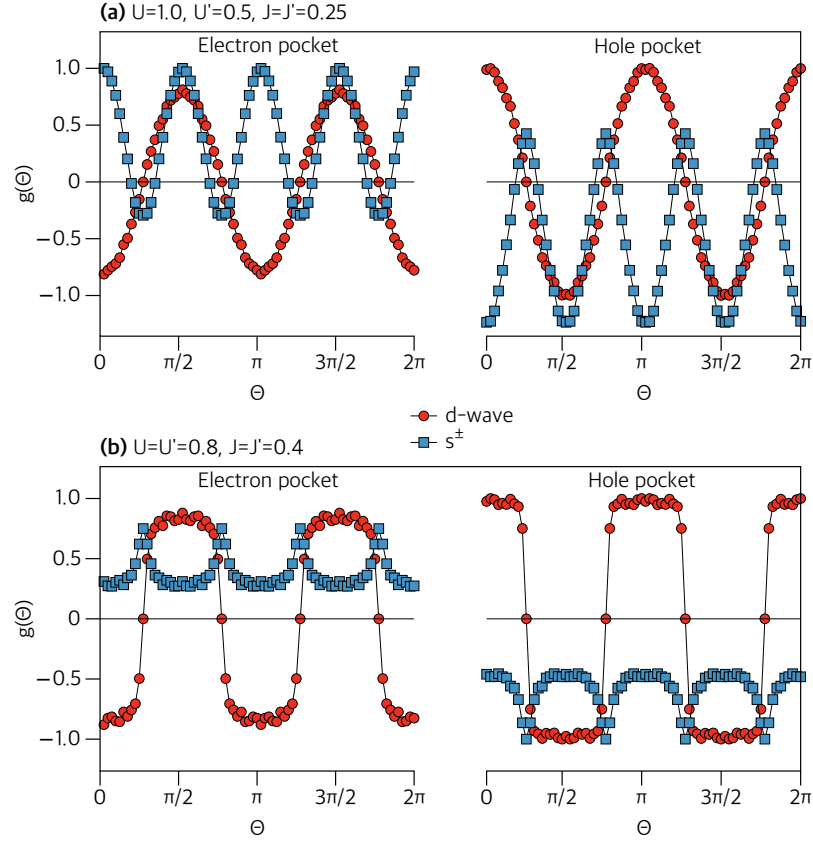


FIG. S3: The pair eigenfunction  $g_d(k)$  and  $g_{s^\pm}(k)$  versus  $k$  around the Fermi surfaces for (a)  $U = 1.0, U' = 0.5, J = J' = 0.25$  and  $T = 0.06$ , and (b)  $U = U' = 0.8, J = J' = 0.4$  and  $T = 0.1$ .